 CMC, vol.1, no.2, pp.153-171, 2004

Prediction of the behavior of RC Beams Strengthened with FRP Plates

Ricardo Perera[1]

Abstract: Epoxy-bonding a composite plate to the tension face is an effective technique to repair reinforced concrete beams since it increases their strength and rigidity. In this paper, the structural behavior of reinforced concrete beams with fibre reinforced polymer (FRP) plates is studied numerically. For it, a numerical damage model is used in order to predict their strength, stiffness and failure modes observed in experimental tests taking into account the influence of different variables such as the amount of steel reinforcement, the type and amount of external reinforcement, the plate length, etc. The consideration of concrete cracking and the yielding of the steel rebars allows to predict in a realistic way the behavior of the strengthened beams and especially the debonding failure mode. In that sense both end and midspan debond can be represented since the model is able to reproduce the tension stiffening phenomenon.

keyword: Fiber reinforced plastics (FRP); strengthening; damage mechanics; reinforced concrete

1 INTRODUCTION

Nowadays, it is needless to emphasize the importance of advanced composite materials for repairing in aerospace [Park, Ogiso and Atluri (1992), Atluri (1997), Wen, Aliabadi and Young (2002)] and civil engineering [Hollaway and Leeming (1999), Teng, Chen, Smith and Lam (2002)]. In particular, in civil engineering, from the first investigations performed in the middle of 80's at the Swiss Federal Laboratory for material testing (EMPA) [Meier, Deuring, Meier and Schwegler (1993)] for the flexural strengthening of RC beams using CFRP plates, fiber reinforced composites are increasingly becoming important in the construction industry because of their advantageous properties not available from other materials [ACI Manual of concrete practice: Part 5 – ACI 440.2R-02 (2003)]. It is of special interest and widespread acceptance the bonding of fiber-reinforced plastic (FRP) plates to critical areas of a concrete beam subjected to tension as an excellent method to increase the flexural and shear strength of the member [Teng, Chen, Smith and Lam (2002)]. This method has many advantages over the traditional techniques since it increases the capacity of the beam altering minimally its dimensions through a material of easy installation (in fact, the work can be carried out while the structure is still in use), high corrosion resistance and with a high strength/weight ratio.

In strengthening reinforced concrete beams with FRP plates, different failure modes have been reported for full composite action. For flexural failure, the ultimate strength of the beam is mainly controlled by rupture of the plate or compression crushing of concrete. This failure mechanism is desirable from a structural performance point of view especially if the rupture of the plate is reached since, in this case, its maximum capacity is used [Hollaway and Leeming (1999)].

However, although the plate bonding technique has many practical advantages, its application can produce also a local failure mode of the strengthened beam by loss of composite action due to the debonding of the composite plate and the beam [Saadatmanesh and Ehsani (1991), Sharif, Al-Sulimani, Basunbul, Baluch and Ghaleb (1994)]. This failure mode is due to high interfacial stresses and occurs suddenly and in a brittle manner and, therefore, it should be avoided since it not only decreases the strengthening potential of externally bonded plates but it is not acceptable from a point of view of structural safety. Debonding occurs commomly in the concrete, adjacent to the adhesive-to-concrete interface, since the weakest point in the bond between the FRP plate and the concrete is in the concrete layer near the surface.

Methods of elastic analysis, traditionally used, predict that peak shear and peel interfacial stresses occur at the plate ends [Malek, Saadatmanesh and Ehsani (1998),

[1] Dept.Structural Mechanics, Technical University (UPM) c/ José Gutiérrez Abascal 2, 28006 Madrid, Spain. Email:perera@estru.upm.es

Ravinovich and Frostig (2000)]. The abrupt termination of the plate can result in a strong concentration of shear and vertical normal stresses which causes the plate to peel off towards the centre of the beam. Therefore, this narrow area close to the bonded plate edge is a very critical part of the strengthened beam. However, when flexural cracking in concrete is considered [Arduini and Nanni (1997), Ravinovich and Frostig (2001)], the distribution of these interfacial stresses changes from that of the elastic phase. In the cracked areas, high stress concentrations originate because of the presence of the FRP plate. As a consequence of it, the local failure mechanism can initiate at any flexural crack, away from the plate ends, and propagates from there to the ends of the plates [Sebastian (2001), Rahimi and Hutchinson (2001)]. Midspan debond is initiated by the transmission of high shear stresses, due to the tension stiffening in the cracked concrete, from the plate through the adhesive to the cover concrete. Other phenomena, like the corrosion of the embedded steel, can contribute also to midspan debond action.

Therefore, the influence of cracking in the concrete beam and phenomena like the steel corrosion have to be considered on the load-carrying capacity and the failure mode of the strengthened member.

The aim of this paper is to investigate the suitability of FRP for externally bonded reinforcement of concrete structures subjected to flexural loading. For it, a good simulation of the stresses at the concrete/FRP interface has to be performed since the failure is governed in many cases by local failure. Many numerical studies proposed in the literature assume a linear elastic behavior for concrete which represent a very limited approach. On the other hand, most of numerical studies [Malek, Saadatmanesh and Ehsani (1998), Ravinovich and Frostig (2001)] considering cracking focus only on the end debond mode in which delamination initiates at the ends of the plate. In this study, a detailed nonlinear FE analysis has been carried out with the purpose of studying the possible critical failure modes considering the influence of parameters such as the amount of internal flexural reinforcement, geometric and material properties of the FRP plate and the RC beam that influence the performance of the strengthened beam. It will help to understand the relationships among these variables and the failure mechanisms associated with these structures.

Since the nonlinear behavior of concrete is dominated by the progressive cracking a damage model is used which allows to take into account the effect of the flexural microcracks on the plate debonding. The model can properly describe the interfacial stress distributions that arise during loading of the RC beam. The model is calibrated through comparison with some experimental results and, then, it is used to investigate the behavior of the strengthened beam and the possible failure modes.

2 ANALYTICAL MODEL

The constitutive laws of the four materials, namely steel, concrete, adhesive and FRP, are considered in the numerical model. The stress-strain relationship of reinforcing steel is assumed to be bilinear. For the FRP plates, a linear elastic relationship up to failure is assumed. The adhesive is considered perfectly linear elastic. This assumption is justified in the case of adhesives for civil engineering use. A non-linear stress-strain relationship based on damage mechanics is assumed for concrete, which is described next.

2.1 Concrete

The nonlinear behavior of concrete under load is controlled by cracking. Computationally, the cracking simulation of brittle structures is performed usually using two procedures: the discrete and the smeared crack approaches. In the first procedure, cracks are incorporated in the model adapting the solid geometry and keeping a linear elastic behavior for the solid. With this model the position and direction of crack growth must be predefined which represents a limiting factor. On the other hand, in the smeared crack formulation the geometry is kept fixed and cracking is considered through the constitutive equations. Cracks are incorporated within a fixed model through a stiffness and strength reduction. In this method, it is impossible to predict local fracture since the crack formation is spread over the entire structure.

More recently, damage models have been used extensively for simulating nonlinearity effects in brittle materials. Introduced for creeping problems [Kachanov (1958)], their use has been extended to simulate the progressive failure observed in some materials such as concrete through the evolution of the mechanical properties of the continuum as microcracking develops. In a damage analysis, a damage variable d is defined to model the local effects of concrete microcracking. This variable,

bounded by 0 and 1, represents the effective surface density of microdefects.

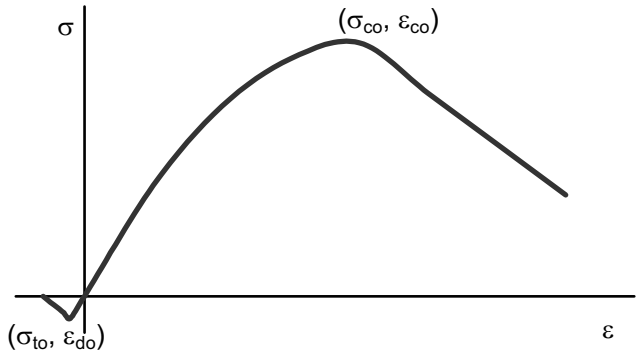

Figure 1 : Concrete response curve for monotonic loading

In this work, an isotropic damage model has been adopted for concrete in order to try to represent accurately the strain-softening response of concrete (Fig. 1) and, moreover, damage values allow to define the progression of microcracks inside the concrete member. Although with an isotropic model all the damage modes cannot be described, its implementation is easier and its results are acceptable without high confining pressure and under loading monotonic [Mazars and Pijaudier-Cabot (1989)], which corresponds to the study performed here.

According to the damage mechanics, the constitutive equations for a damaged material are formulated through the strain equivalence principle [Lemaitre (1996)]:

$$\sigma = (1-d)D^e : \varepsilon^e \tag{1}$$

where σ is the Cauchy stress tensor, ε^e the strain tensor and D^e the isotropic elastic moduli.

To define completely the constitutive equation (1) it is necessary to specify a damage evolution law.

For it, the Mazars isotropic damage model [Mazars and Pijaudier-Cabot (1989)] has been adopted. In this model, degradation in both tension and compression is allowed and its formulation is performed according to the thermodynamics of irreversible processes. For it, in order to check if damage occurs, it is necessary to define a loading surface. The loading surface used is based on the criterion of maximum principal strain and is given by

$$f(\varepsilon, \varepsilon_{do}) = \tilde{\varepsilon} - \varepsilon_{do} \tag{2}$$

where ε_{do} is the threshold value above which damage occurs, $\tilde{\varepsilon}$ is the equivalent strain which is defined as

$$\tilde{\varepsilon} = \sqrt{\sum_{i=1}^{3} \left(\langle \varepsilon_i \rangle_+ \right)^2} \tag{3}$$

where ε_i are the principal values of ε.

In Eq.(2), when $\tilde{\varepsilon} > \varepsilon_{do}$ damage starts growing. If damage occurs, two types of damage are considered, one for tension (d_t) and other for compression (d_c). The total damage is the weighted sum of both of them:

$$d = \alpha_t d_t + \alpha_c d_c \tag{4}$$

the weights α_t and α_c being functions of the strain state defined by the following expressions [Mazars and Pijaudier-Cabot (1989)]:

$$\alpha_t = \sum_{i=1}^{3} H_i \frac{\varepsilon_{ti}(\varepsilon_{ti}+\varepsilon_{ci})}{\tilde{\varepsilon}^2} \qquad \alpha_c = \sum_{i=1}^{3} H_i \frac{\varepsilon_{ci}(\varepsilon_{ti}+\varepsilon_{ci})}{\tilde{\varepsilon}^2} \tag{5}$$

where

$$H_i = \begin{cases} 1 & if \quad \varepsilon_{ti}+\varepsilon_{ci} \geq 0 \\ 0 & if \quad \varepsilon_{ti}+\varepsilon_{ci} < 0 \end{cases} \tag{6}$$

and ε_t ,ε_c the strain tensors associated to the positive and negative principal stresses, respectively.

In addition to the loading surface it is necessary to define two damage evolution laws, one for tension damage and the other for compression damage. These laws are chosen through an expression that describes the stress-strain curve for uniaxial tensile and compression tests performed on concrete specimens when damage initiates which occurs when $\tilde{\varepsilon} \geq \varepsilon_{do}$. The expression of this curve is as follows [Mazars and Pijaudier-Cabot (1989)]:

$$\sigma = E \left[\varepsilon_{do}(1-A) + \frac{A\tilde{\varepsilon}}{\exp\left[B(\tilde{\varepsilon}-\varepsilon_{do})\right]} \right] \tag{7}$$

where A=A_c and B=B_c characterize the compression behaviour and A=A_t and B=B_t characterize the tensile behaviour and they depend, therefore, on each particular concrete. It must be noted that for the tensile test, $\tilde{\varepsilon}$ coincides with the uniaxial strain, while for the compression test $\tilde{\varepsilon}$ is obtained from the transverse tensile strains induced by the uniaxial compression strain; ε_{do} is the uniaxial tensile strain from which a decrease in the stiffness appears.

Comparison between Eqs (1) and (7) for uniaxial tension and compression allows the identification of the damage laws for tension and for compression, respectively.

3 PLATE DEBONDING

Generally, brittle failure modes fall into two groups: those initiated by delamination of concrete cover near flexural cracks in the midspan area of the repaired beam and those in which concrete delamination progresses from the ends of the plates inwards.

Midspan debonding is dominated by high shear stresses concentrations around flexural cracks. When these stresses exceed the strength of the weakest material, usually concrete, local debonding occurs by propagation of an horizontal crack in the concrete adjacent to the adhesive-to-concrete interface towards the plate end. This situation is very similar to that observed in simple shear tests.

On the other hand, debonding starting from the plate end is believed to be controlled by the interfacial shear and normal stresses [Malek, Saadatmanesh and Ehsani (1998)] although, from the theory proposed by Täljsten (1997) , it has been verified [Zarnic, Gostic, Bosiljkov and Bokan-Bosiljkov (1999)] that, for sufficiently thin plates, the influence of normal stresses is very small. Previous analytical approaches [Roberts (1989); Malek, Saadatmanesh and Ehsani (1998)] have proposed a debonding prediction model based on the shear and normal stresses concentrations at the plate cutoff end. These models appear to be too complex for the practical day-to-day design. Due to it, a new practical design approach using the interface shear stress as the primary criterion has been proposed recently to predict local debonding failure in a strengthened RC beam [Mukhopadhyaya and Swamy (2001)]. Through the analysis of various published experimental data, it has been found that the end debonding can be also controlled by a limiting interface shear stress. This approach constitutes a promising design criterion and, therefore, it will be used in this study.

The interfacial shear stress between FRP plate and adhesive can be calculated by equilibrium of an infinitesimal part of the FRP plate. The following equation is obtained [Malek, Saadatmanesh and Ehsani (1998)]

$$\tau_p = t_p \frac{d\sigma_p}{dx} \tag{8}$$

where τ_p is the shear stress and t_p, σ_p are the thickness and the axial stress of the plate, respectively, and x is the distance along the plate.

According to Eq.(8), local shear failure will initiate in areas where high axial stress gradients in the plate appear which occurs near concrete flexural cracks (midspan debonding) or at the plate ends (end debonding). The possibility of one failure mode occurring over the other is dependent on many factors and it will be studied in the next sections.

4 PARAMETRIC STUDY

4.1 Materials and geometry

A parametric study was conducted on the behavior of simply supported reinforced concrete beams strengthened with FRP plates under four-point bending (Fig. 2). Due to the symmetry of the beam, only half of the beam was analyzed with appropriate constraints at the centerline. For 2D analysis, concrete beams and FRP strips were modeled with four-noded quadrilateral isoparametric elements. The adhesive layer was modeled with a single row of four-noded elements. For the internal rebars, two-noded bar elements smeared onto the concrete elements were used. Finer mesh discriminations were made at the vicinity of the plate ends and at intermediate regions since the largest stress concentrations can occur at those areas. A typical mesh definition of the test beam is shown in Fig. 3.

In the study, different parameters were considered to study the behavior of the repaired RC beam. Firstly, we took in consideration the parameters affecting the geometry and properties of the non repaired RC beam. For it, two rectangular beams (beams A and B) with different cross sections (Fig. 2) were considered (Table 1). The shear span to depth ratios for both beams are 4.36 and 6.19 , respectively. The reference beam A, except in the length of the FRP strip, is that tested at the University of Arizona, Tucson, and described in Saadatmanesh and Ehsani (1991).

To study the effect of the original reinforcement ratio on the strength of repaired beams, two different amounts of steel reinforcement were considered, S1 and S2. The first corresponds to a high steel reinforcement ratio for the considered beam sections while the second is characteristic of underreinforced beams which require strengthening. The shear reinforcement is maintained constant. The reinforcement details of the beams are summarized

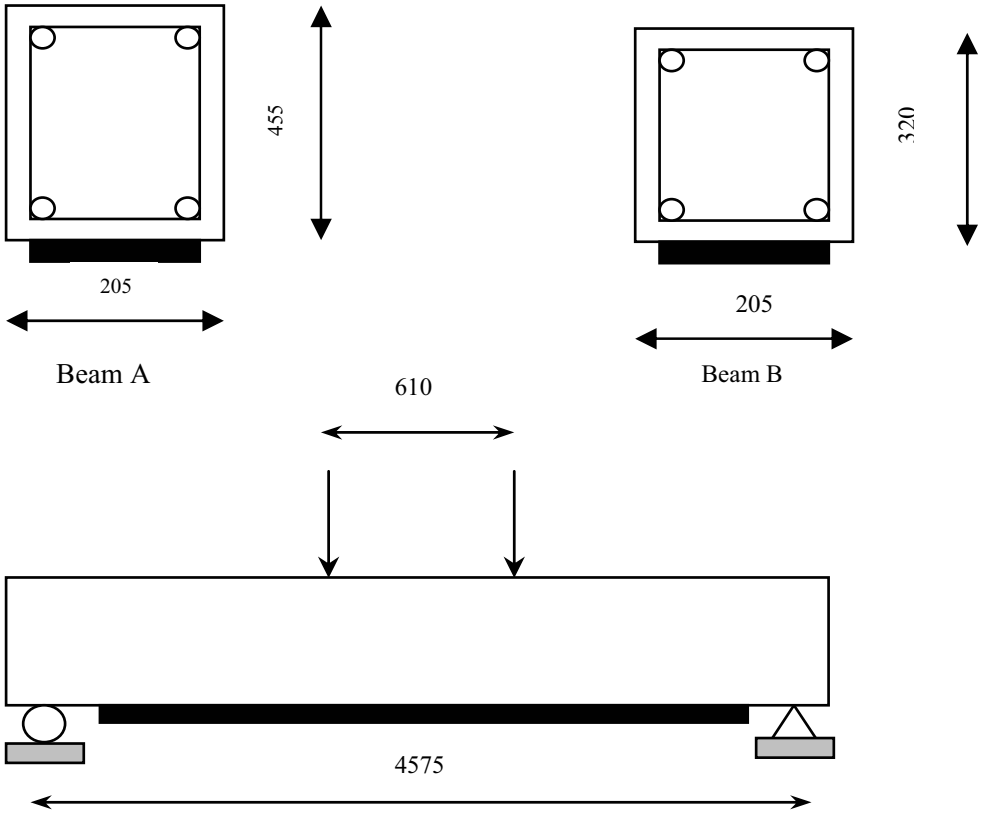

Figure 2 : Details of the geometry of the RC beams

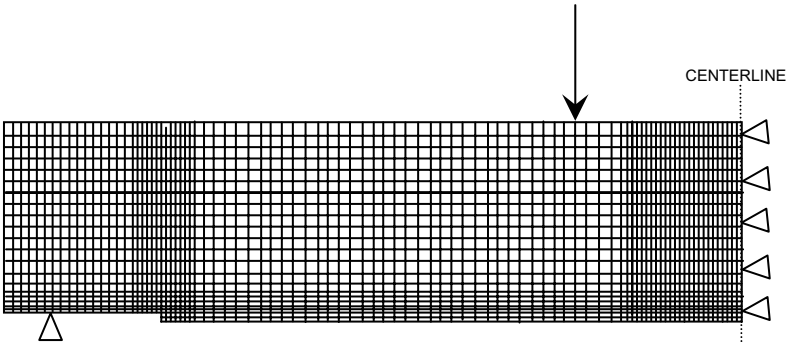

Figure 3 : Typical 2D FE model of RC beam with FRP plate

Table 1 : Geometry of the beams

Beam		*h*x*b* (mm^2)	L (mm)	L_{FRP} (mm)
A	A1	455x205	4575	4175
	A2			4475
B	B1	320x205	4575	4175
	B2			4475

Table 2 : Steel reinforcement details of specimens

Steel reinforcement	Tension	Compression	Number of stirrups
S1	2ϕ25mm	2ϕ13mm	34ϕ13mm@150mm
S2	2ϕ10mm	2ϕ8mm	34ϕ13mm@150mm

Table 3 : Mechanical properties of FRP and adhesive

Material		E (MPa)	f_t (MPa)	Thickness (mm)
GFRP	FRP1	37230	400	6
	FRP2			2
CFRP	FRP3	165000	2800	6
	FRP4			2
Adhesive	AD	814		1.5

in Table 2.

The average compressive strength specified for these beams was 35 MPa and the average measured yield stress of the bars was 456 MPa.

For the strengthening, two different FRP materials were considered (Table 3). Firstly, GFRP plates with an average modulus of elasticity of 37230 MPa and an average ultimate strength of 400 MPa and, secondly, CFRP plates with values of 165000 MPa and 2800 MPa, respectively. The thickness of both FRP plates was varied from 0.002 m to 0.006 m . Two different lengths of the FRP plate were considered, 4.175 m to 4.475 m.

For the adhesive (Table 3), epoxy was used with a modulus of elasticity of 814 MPa. The adhesive thickness, although not specified in the original source, was taken equal to 1.5 mm according to the value specified in Malek, Saadatmanesh and Ehsani (1997) for the same specimens; in any case, this is a parameter difficult to control on site.

4.2 Calibration of the analytical model

Before beginning the parametric study, it was necessary to select the unknown parameters, A_t, B_t, A_c and B_c, defining the damage model. These values are obtained from the properties of concrete. The Young's modulus and the compressive strength are known. However, the concrete tensile strength is, usually, unknown and the numerical results can be particularly sensitive the value used. For it, the proposed numerical model was calibrated with experimental tests reported by Saadatmanesh and Ehsani (1991). The beam A-S1-FRP1 with a plate length of 4.26 m, corresponding to one of the experimental tests, was adopted for comparison.

After some numerical tests and comparing the load-deflection curves with the results from the experimental test, the most accurate numerical solution was obtained with a concrete tensile strength of 3.5 MPa which was, therefore, adopted for the calculations.

The best numerical prediction of the load-deflection response of the strengthened beam along with the experimental results is shown in Fig. 4. Although, the numerical model underpredicts the strength compared to the ex-

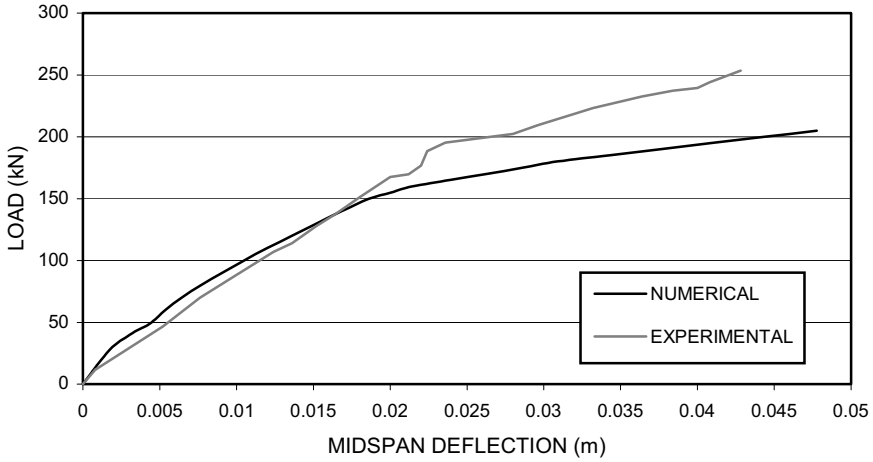

Figure 4 : Load versus deflection (beam A-S1-FRP1)

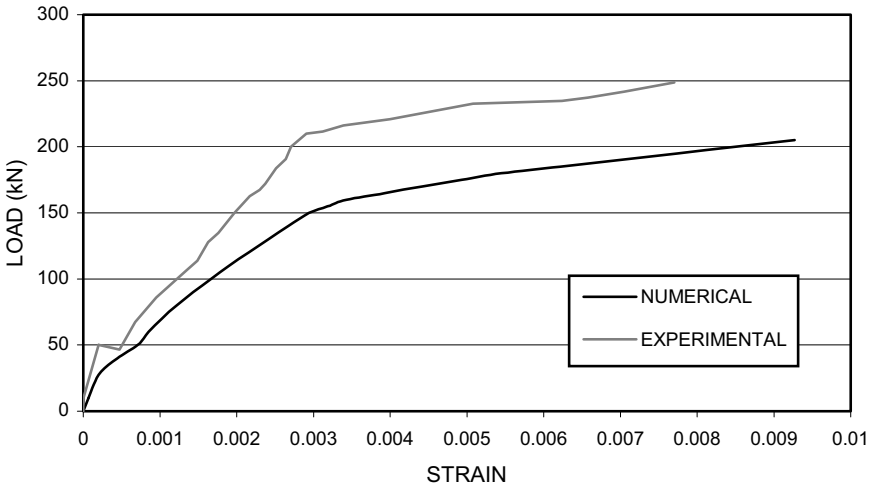

Figure 5 : Load versus strain in steel rebars (beam A-S1-FRP1)

perimental test, an acceptable agreement can be observed between both results. The reduction of the stiffness of the beam after the first microcracks was perfectly represented by the model. However, in the numerical model the steel rebars yielded at 155 kN while in the experimental results yielding was reached at 185 kN; the numerical model yields a less stiff structure specially after the yielding. Such discrepancies are due to some assumed properties used in the model, such as the stress-strain relations in the concrete and the reinforcement steel hardening.

Fig. 5 shows the numerical and experimental load versus strain curves in steel rebars. After cracking of concrete, the strain in the steel rebars increased and the stiffness of the beam reduced which is represented by the model. Then, the strain increases linearly until the steel rebars yield.

In Fig. 6, the measured and calculated load versus strain in the composite plate are shown. The higher rate in the strain increment in the plate after the cracking and after the steel rebars yielding are reflected also in the numerical model.

With the purpose of evaluating the validity of the model for other different specimens, comparisons were done for other set of experimental data available in literature. In particular, beams B6 and B8 reported by Rahimi and Hutchinson (2001) were taken for comparison. The beams were 2.3-m long x 0.2-m wide x 0.15-m deep with a medium internal reinforcement ratio. Beam B6 was externally reinforced with a CFRP plate with the follow-

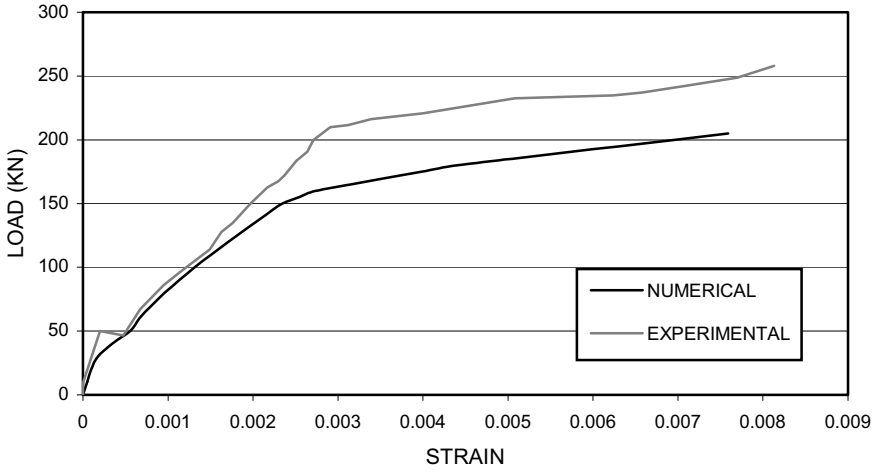

Figure 6 : Load versus strain in FRP plates (beam A-S1-FRP1)

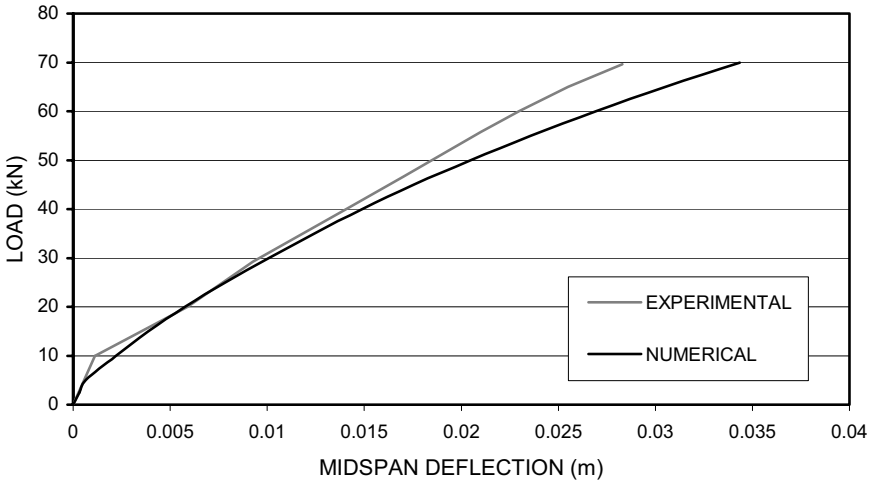

Figure 7 : Load versus deflection for beam B6

ing values: E=127000 MPa and strength=1532 MPa. On the contrary, beam B8 was externally reinforced with a GFRP plate with the following values: E=36000 MPa and strength= 1074 MPa. The concrete compressive strength was of 54-69 MPa and the same value of 3.5 MPa was adopted for the tensile strength. Figs. 7 and 8 show the comparison between the numerical and experimental load-midspan deflection curves for the beams B6 and B8, respectively. The agreement between both curves can be considered good enough, specially for the beam with a higher stiffness plate, and the maximum strength was predicted by the numerical model. A variation appears between both curves after the first yielding of the steel reinforcement since no steel hardening was considered for the numerical model. From the results, it can be concluded that a value of 3.5 MPa for the concrete tensile strength provides also in this case a good correlation with the experimental results and, therefore, it will be adopted in the calculations.

4.3 Design flexural strengthening

Previously to perform all the numerical analysis, a step-by-step procedure as recommended in ACI Manual of concrete practice:Part 5 – ACI 440-2R-02 (2003) was performed on the beams studied in the previous section to determine the design flexural strength. The following assumptions were made: Plane sections before loading remain plane after loading; there is no relative slip be-

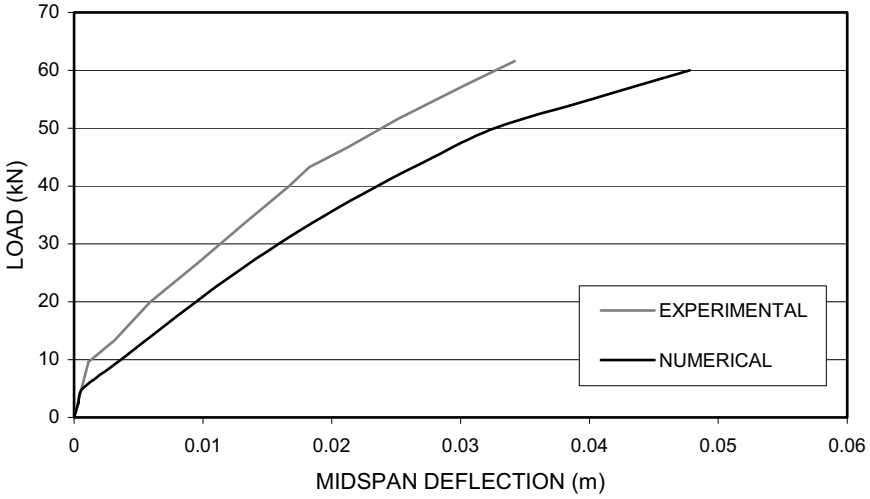

Figure 8 : Load versus deflection for beam B8

tween FRP plate and the concrete; the contribution of the adhesive layer is neglected; the ultimate concrete compressive strength is 0.003; the tensile strength of concrete is neglected and the FRP reinforcement has a linear elastic stress-strain relationship to failure.

In addition to the typical failure modes, FRP debonding is also considered in ACI Manual of concrete practice:Part 5 – ACI 440-2R-02 (2003) through a bond-dependent coefficient.

From the step-by-step analysis, the predictions of the ultimate load for the three analyzed beams previously, A-S1-FRP1, B6 and B8, reached values of 121.5, 45 and 33 kN, respectively, and the maximum strength was limited by the FRP debonding in the three cases. Compared to the experimental results (Figs. 5, 7 and 8), the closed-form solutions underestimated the strength of the beams.

4.4 Strength

With the parameter values of the damage model determined previously through the calibration of the beam A-S1-FRP1, a parametric study was performed in order to consider the influence of different variables (geometric and material properties) on the performance of FRP soffit-plated RC beams. In Figs. 9, 10, 11 and 12 numerical results for the specimens A and B are shown in terms of applied load-midspan deflection.

It can be observed from these figures that all beams with FRP reinforcement performed better than the unplated beams in terms of strength. The strength increase is strongly influenced by the amount of external reinforcement and the FRP stiffness. When the strengthening is performed with CFRP plates, for the type S1 beams, with a high conventional reinforcement ratio, the effectiveness of bonded external reinforcement, in terms of ultimate load of the repaired beam and ultimate load of the unrepaired beam, is not so evident when comparing with beams with a lower internal reinforcement ratio, specially for type A beams. In case of shallower beams (type B beams) the strength increase provided by the external reinforcement is more evident even in beams with a higher steel reinforcement. When CFRP plates are used, the strengthening technique is, therefore, particularly effective for beams with relatively low steel reinforcement ratios which is natural since only underreinforced beams require strengthening. In general, the two main consequences of flexural strengthening of RC beams using CFRP plates with a high axial stiffness are the strength gain and the ductility reduction. In general, ductility is refered to the ability of a RC section to sustain its peak strength capacity over a range of displacements which occurs after the first yield in the steel rebars since, then, the response stiffness is very small. On the contrary, for RC beams strengthened with FRP plates, after yielding of steel reinforcement the stiffness is also considerable due to the elastic contribution of the strengthening plate. In spite of it, ductility can be defined in an a rough way as the ratio between the ultimate displacement and the displacement corresponding to the first yielding of the steel reinforcement.

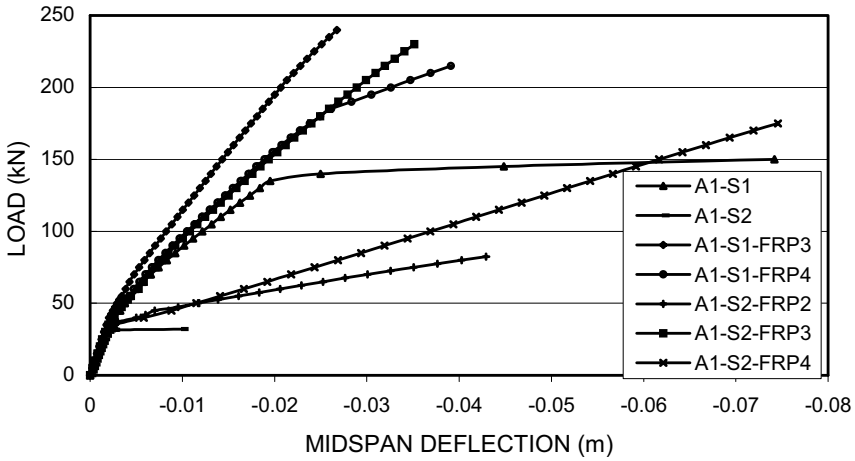

Figure 9 : Load-deflection behavior (Type A1 beam)

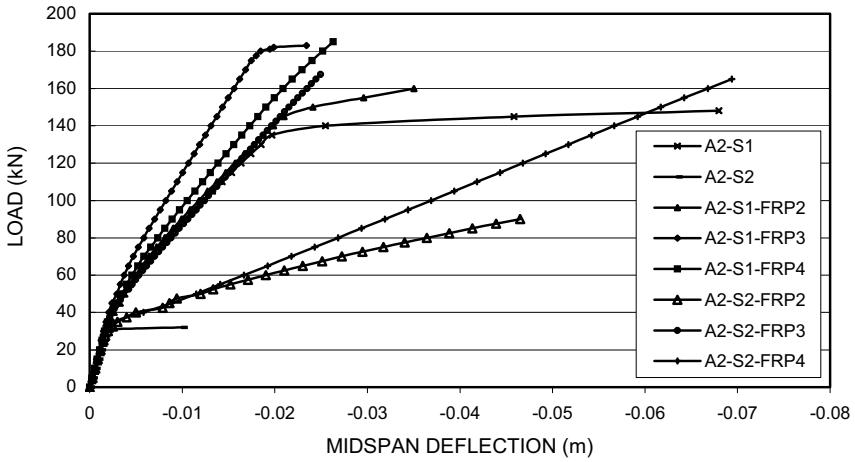

Figure 10 : Load-deflection behavior (Type A2 beam)

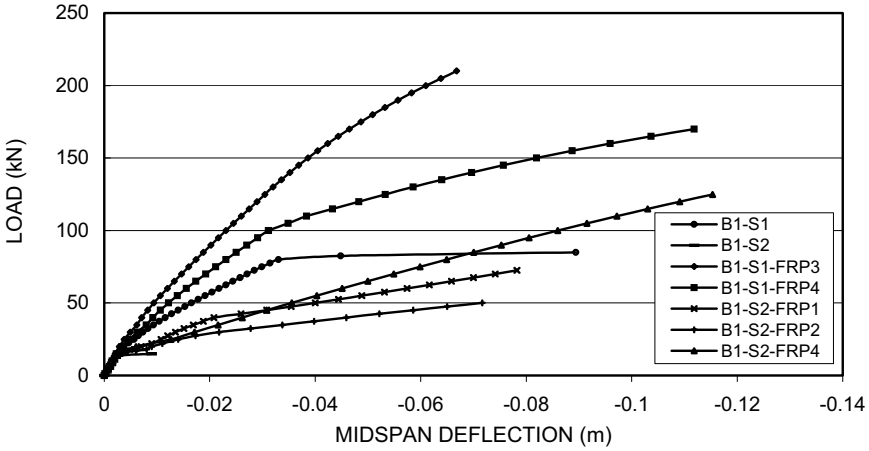

Figure 11 : Load-deflection behavior (Type B1 beam)

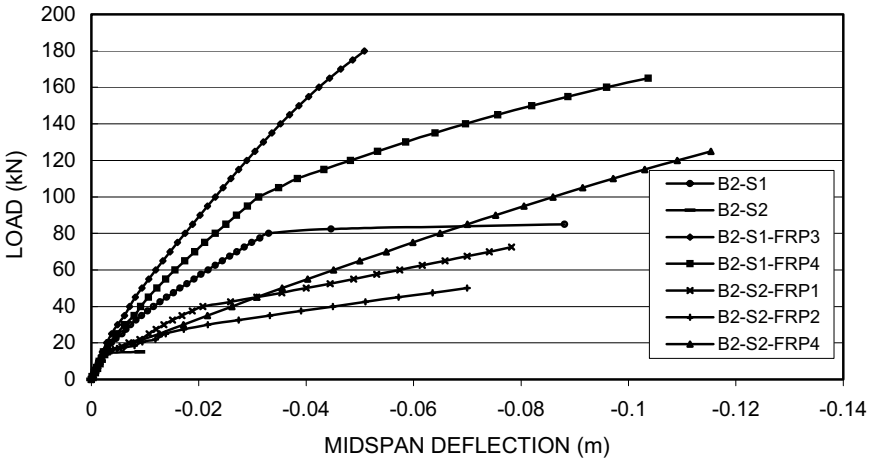

Figure 12 : Load-deflection behavior (Type B2 beam)

Small cross-sectional areas of external CFRP increase significantly the failure load. However, this strength increase can be accompanied by a change of the failure mode from ductile to brittle because of the plate debonding which is undesirable since the failure is sudden with no or very little warning. To avoid this, the ductility index should exceed a certain value. In general, the higher the FRP stiffness and its thickness, the higher the strength improvement but the lower the ductility and vice versa. Because of it, a compromise must be reached between both of them. According to the ACI Manual of concrete practice: Part 5 – ACI 440-2R-02 (2003), adequate ductility is achieved if the strain in the steel at the point of failure is as least 0.005. If not, a higher reserve of strength must be provided.

When plates with low elastic modulus, such as GFRP plates, are used for strengthening the same conclusions are not obtained. Even for type S2 beams the influence of the GFRP plates is not so important in terms of strength. For this type of strengthening, using plates with a low elastic modulus, the strength increase is accompanied by a strong displacement increase reaching the ultimate load in a ductile way. The axial stiffness of the FRP plate is low and can be insufficient to limit the deflections of the plated beams. This phenomenon is important since non acceptable deflections can be reached under service loads. In most of these cases the typical failure mode is rupture of the FRP plate which occurs following the yielding of the longitudinal steel bars. Yielding of steel, which is characterized by the change of the slope, is clearly apparent when low stiffness plates are used, differently to high stiffness plates where only a slight change occurs. The failure strain is, usually, higher than when using CFRP. When the modulus of elasticity of FRP is low, its thickness has to be higher to obtain a strength improvement. The same remark can be made for beams with a low steel ratio strengthened with FRP4 plates. Their lower thickness compared to FRP3 plates implies more ductility and less strength. In general, more ductile behavior is observed in shallower beams and beams strengthened with FRP plates of low axial stiffness $E_{FRP}A_{FRP}$. A higher ratio between ultimate load of the reinforced beam and the ultimate load of the RC one is also observed for shallower beams.

4.5 Stiffness

From Fig. 9, 10, 11 and 12 it is clear that FRP plates do not produce an increase in stiffness in the elastic range of the beams . When cracking of beams initiates the increase in stiffness for plated beams compared with unplated beams is clear and the effect is even more evident when steel yields indicating that , at this point, practically the composite plate alone resists further increments of the tensile component of the moment. However, as it is expected, the postcracking stiffness increase is strongly dependent on FRP stiffness and the amount of internal reinforcement. In general, in beams plated with GFRP plates, high deflections can be reached under service loads which is an important factor to consider in the design. The same phenomenon occurs for RC beams with low steel reinforcement (S2) and strengthened with FRP4 plates; the postcracking stiffness is not very high

since the steel and FRP4 stiffnesses are not very high. However, with high steel reinforcement (S1) or when the internal reinforcement is low (S2) but the RC beam has been strengthened with FRP3 plate the postcracking stiffness decrease is very low.

On the other hand, the beam stiffness after the steel begins to yield is dependent on the relative stiffness between FRP plate and that provided by steel reinforcement in tension. When the stiffness provided by the external reinforcement is high, the effect of steel yielding on the load-deflection response is low since the contribution of the strengthening plate is still considerable after the yielding. However, when the plate stiffness is considerably lower than the stiffness provided by the internal reinforcement in tension the drop in the global stiffness after the steel yielding is more evident , especially for shallower beams. It is the case of S1 beams strengthened with FRP1, FRP2 and FRP4 plates.

4.6 Variation of Stresses in Steel Reinforcement, FRP Plates and Concrete/External Plate Interface

A benefit of the nonlinear damage analysis of the strengthened beam is the ability to examine the local behavior at the adhesive-concrete interface considering flexural cracking of the RC beam. The influence of cracking in the concrete beam is essential on the distribution of the interfacial stresses and therefore on the failure mode of the repaired beam. As is is well known, in RC beams the tension stiffening, caused by the bond between the tension reinforcement and the cracked concrete, is a source of axial stress gradient in the rebars. The same phenomenon must also occur in the FRP plate bonded onto the cracked concrete. Taking into account that shear bond stresses are generated by axial stress gradients in the plate (Eq. 8), tension stiffening produces high shear bond stresses at the midspan which are transmitted to the concrete through the adhesive. Elastic numerical models cannot represent the natural nonlinearities (concrete damage) and they always predict maximum stresses at the plate ends [Malek, Saadatmanesh and Ehsani (1998)]. However, with a concrete damage model it is possible to represent the effects due to flexural cracking.

The distribution of interfacial stresses is very complex and, therefore, such as it was remarked in previous sections, many factors influence the possibility of occurring end peel failure mode or midspan debond. Among them, three factors are considered: the FRP plate stiffness, the plate length and the shear span-beam depth ratio.

In order to study the influence of the plate stiffness on the interfacial stress distribution, the shear distribution at the adhesive-concrete interface as a function of the position along the beam axis is shown in Fig. 13 at the maximum load level for different beam types. As it was commented in a previous section, an interface shear stress criterion has been used to predict plate debonding. In all the figures shown in this section, a limiting interfacial shear stress value of 1.5 MPa has been obtained at the concrete-plate interface beyond failure occurs. It can be observed that stiffer plates attract higher shear stresses at the plate ends encouraging the end peel; with less stiff plates (GFRP plates or CFRP plates with low thickness) peak shear stresses tend to occur near midspan where concrete cracking appears.

Related to the plate length (Fig. 14), when FRP is located far from supports (A1 and B1 beams) the end peel mode is encouraged (predominant) since higher axial stress gradients are produced at the plate end and therefore the end shear stress is also higher. However long plates (plates located near the supports) (A2 and B2 beams) tend to minimize end peel. This phenomenon can be observed in Fig. 14 for type A1-S2-FRP4 and A2-S2-FRP4 beams and for type B1-S2-FRP4 and B2-S2-FRP4 beams. The shear stress distribution is practically similar for beams of the same type except at the plate ends where the values of shear stress increase with the distance of the plate free end from the beam supports.

Another important parameter to take into account is the shear span to beam depth (a/h) ratio. There exists a strong dependence between the shear stress distribution and the a/h ratio (Fig. 13 and 14). Two different ratios have been considered, 4.36 for type A beams and 6.19 for type B beams. With type B beams, end interfacial shear stresses are higher while shear stresses are lower at intermediate regions. Therefore, shallower beams tend to maximize end peel tendencies.

Although, at low load levels, when concrete has not cracked, the peak shear stresses occur at the plate ends, as expected, when load increases the distribution changes and the location of the peak shear stress can move towards intermediate regions depending on factors as those enumerated previously. With the purpose of investigating the changes in interfacial shear stress when the concrete flexural cracks propagate, in Fig. 15, 16 and 17 and Figures 18, 19 and 20, the predicted variation of axial stress

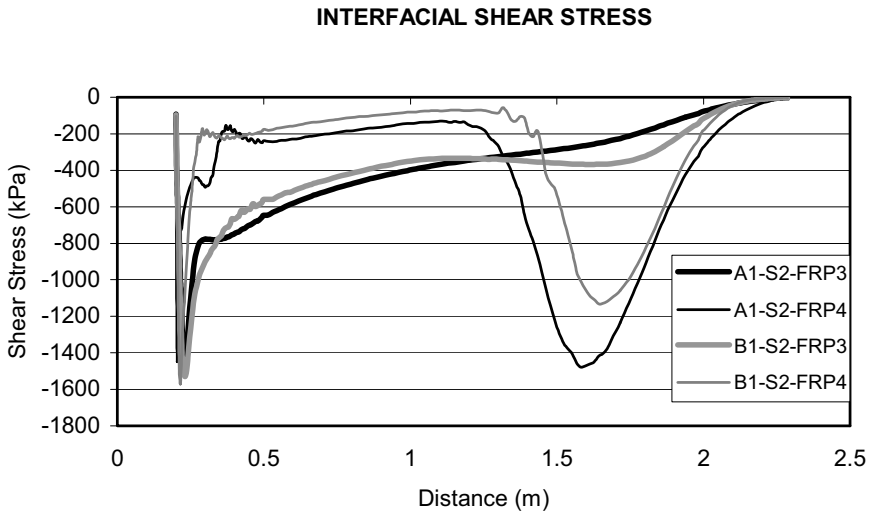

Figure 13 : Interfacial shear stress distribution (Influence of the plate stiffness)

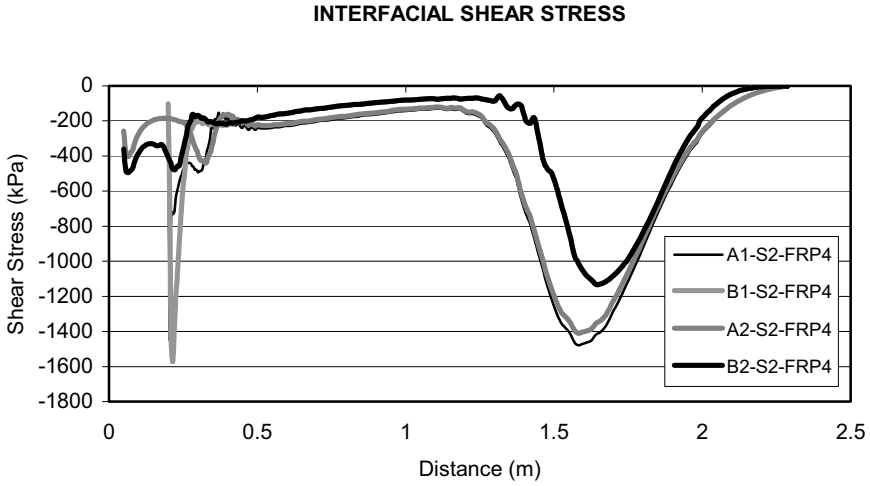

Figure 14 : Interfacial shear stress distribution (Influence of the plate length

with applied load for type A1-S2 and B1-S2 beams with FRP4 external reinforcement along the tensile steel reinforcement and the FRP plates as well as the interfacial shear stress evolutions are shown. As it is expected the largest strains in the steel rebars and FRP plates occurred at midspan of the beams. The numerical damage distribution at the tension face of concrete obtained with the proposed model is also represented for both cases (Fig. 21 and 22). This distribution is very important since it shows where concrete cracks initiate and how they propagate which is essential to consider the stiffening effect and its influence on the shear stress distribution. In general, from the figures, for this damage model the highest gradients of stress at the internal and external reinforcements appear when the damage reaches a value of, approximately, 0.7 and, therefore, it can be assumed that this value represents concrete cracking. Observing the damage distribution for different levels of load and comparing with the curves shown in Fig. 15 and 18, in regions where damage reaches a high value (cracking regions) axial stress gradients in the steel reinforcement appear along the loading process. In these regions, the axial stress in the FRP plate increases at a much faster rate indicating the major contribution of the composite plate to resist tensile stress in areas affected by the damage since part of the tensile stresses released by the cracked

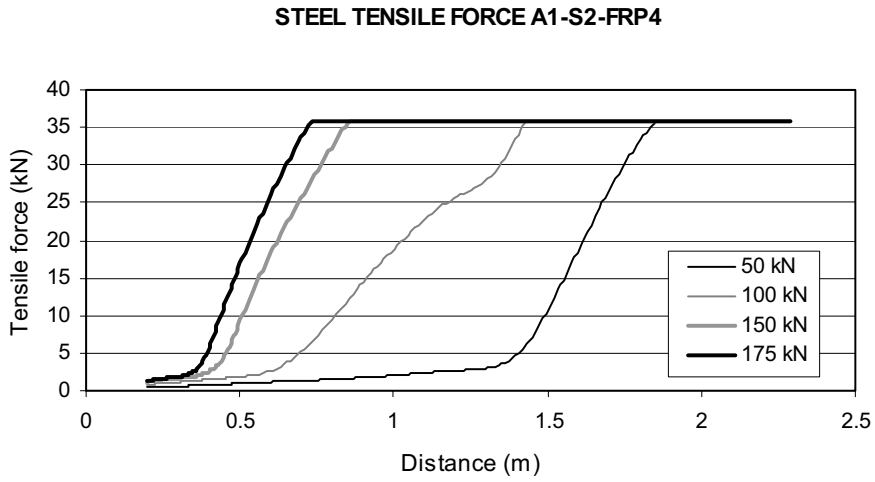

Figure 15 : Variation of axial force along the tensile steel rebar (A1-S2-FRP4)

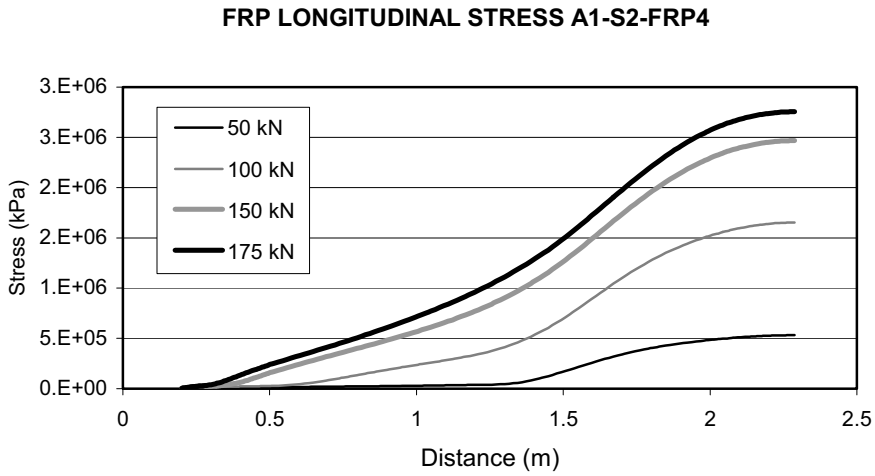

Figure 16 : Variation of axial stress along the external plate (A1-S2-FRP4)

concrete are transferred to the FRP plate. These stresses decrease away from the crack zone. Therefore, the location of the highest axial stress gradients is consistent with the areas where damage reaches the maximum value. In any case, the axial stress gradients in the plate induce through the adhesive, for equilibrium, high shear bond stresses (Fig. 17 and 20) which can produce, as the applied load increases, midspan debond depending on some factors such as it was studied previously. For it, when the interfacial shear stresses reach a critical value, debonding initiates around the crack causing the failure of the beam by propagation towards one of the plate ends. In the Fig. 15, 16 and 18, 19 it can be observed also that when steel yields, another source of axial stress gradient originates in the FRP plate by the same reason as before. It locates in the section where the bottom steel rebars yield and moves to the left as the load increases because of the yield penetration. However, by the same reasons indicated in previous sections, the magnitude of these gradients is dependent on the relationship between the FRP stiffness and the steel reinforcement stiffness.

In both cases (A1-S2-FRP4 and B1-S2-FRP4) the maximum intermediate shear stress appears near the loading point due to the sudden drop in the plate tensile force outside the region of constant moment since a distributed damage model has been used and, therefore, the tension stiffening in the region of constant moment cannot be represented. Such analysis implies that the consideration of a discrete model is not able to represent local

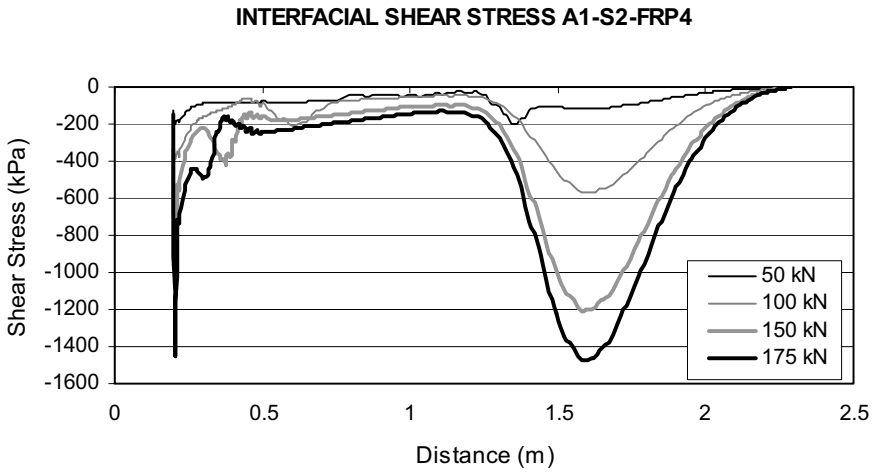

Figure 17 : Variation of shear stress distribution along the concrete/FRP plate interface (A1-S2-FRP4)

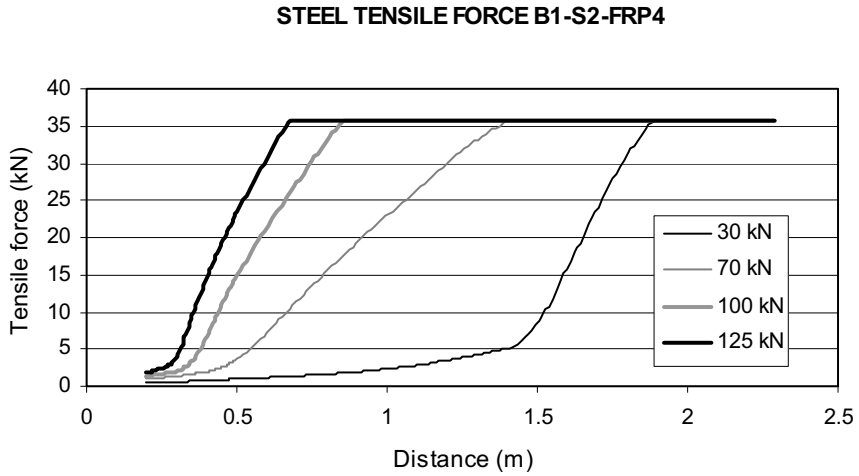

Figure 18 : Variation of axial force along the tensile steel rebar (B1-S2-FRP4)

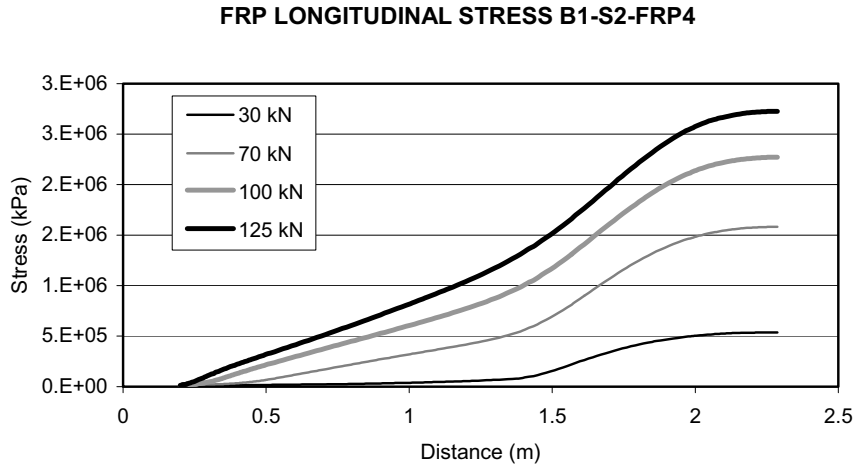

Figure 19 : Variation of axial stress along the external plate (B1-S2-FRP4)

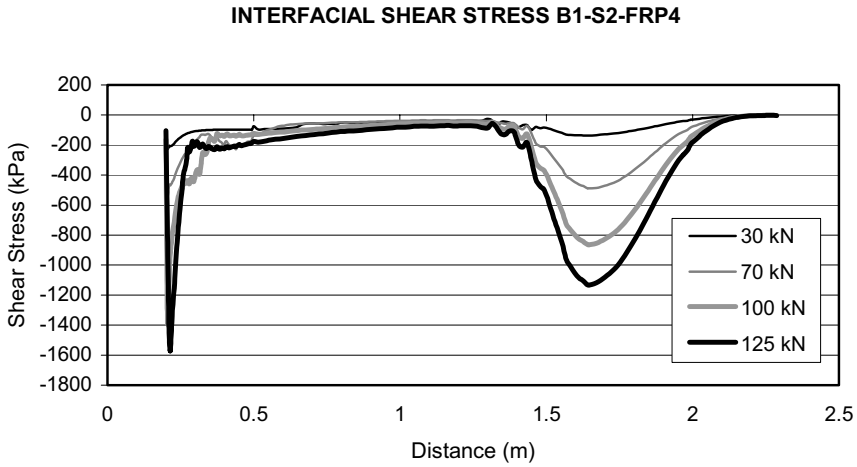

Figure 20 : Variation of shear stress distribution along the concrete/FRP plate interface (B1-S2-FRP4)

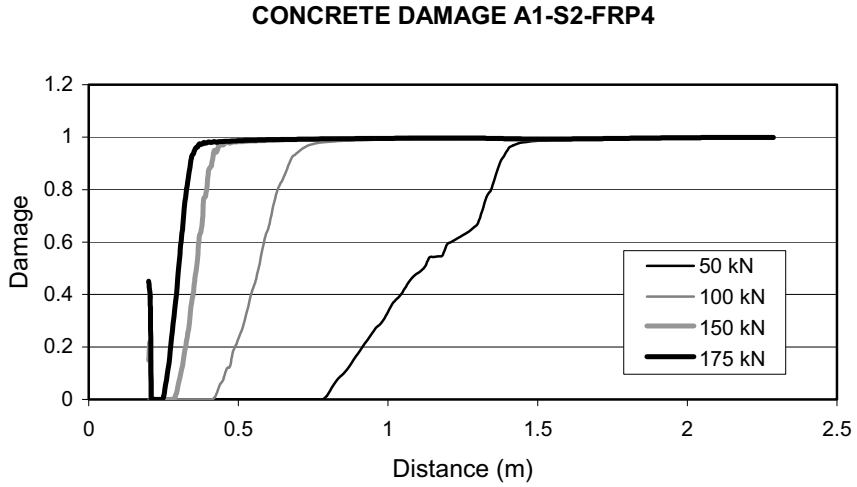

Figure 21 : Variation of damage distribution (A1-S2-FRP4)

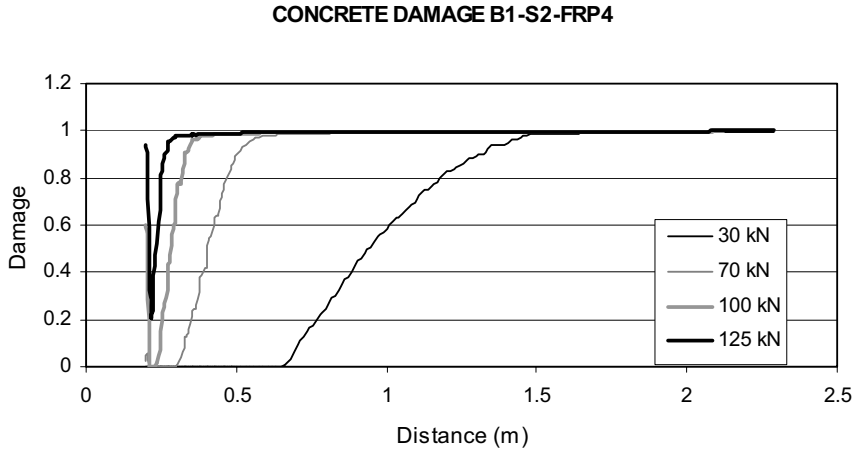

Figure 22 : Variation of damage distribution (B1-S2-FRP4)

microcracks in the area of constant moment. However, in spite of this limitation, the model is perfectly suitable to show if midspan debond can become critical since, in fact, experimental tests have shown that many flexural cracks form in the midspan region of a concrete beam and, therefore, the exact location of initiation of debonding cannot be predicted.

4.7 Corrosion

FRP plates have been also used as a rehabilitation technique for corroded reinforced concrete beams. This aspect has to be considered since steel corrosion can become an important source of high stress gradients in the plate and, therefore, can affect to the serviceability of the structure.

Corrosion, which is more pronounced near the flexural cracks, decreases rebar area inducing by equilibrium high axial stresses and, then, according to Eq. (8), high interfacial shear stresses.

To simulate numerically the reinforcement corrosion effect, the areas of the tensile steel bars were reduced over short lengths in the vicinity of midspan region. Obviously, this is only a simplification suitable for this study since the corrosion induces also hoop stresses in the cover region which have not been considered. Concretely, the tensile rebar diameter was reduced from 10 mm to 8 mm over a length of 0.1 m. To evaluate its effect on the strength and the debonding mode of the strengthened RC beam two types of beams were studied: one, type A1-S2-FRP3 beam, corresponds to a strengthening with a FRP plate of high axial stiffness in which debonding is initiated at the end of the plate; the other beam, type A1-S2-FRP4 beam, corresponds to a beam strengthened with a FRP plate of less axial stiffness in which debonding initiates at an intermediate region.

For the type A1-S2-FRP3 beam the effect provided by the steel corrosion can be neglected since the maximum strength and a interfacial shear stress distribution similar to the case of no corrosion are obtained. However, for the type A1-S2-FRP4 beam, for the assumed limiting shear stress value, the steel corrosion decreases the maximum strength reached by the beam. When corrosion does not exist a maximum value of 175 kN is reached while in case of corrosion this value is only 120 kN. Representing the interfacial shear stress distribution in both cases for the maximum strength (Fig. 23), we can observe that corrosion tends to decrease the shear stress value at the plate end while at midspan areas, where corrosion concentrates, higher values are obtained.

Therefore, we can conclude that the effect of steel corrosion is especially important in those beams for which midspan debond occurs.

5 CONCLUSIONS

The analytical studies performed on concrete beams strengthened with FRP plates indicate that this strengthening method can be used to increase effectively the strength and the stiffness of underreinforced beams. To perform the study a concrete damage model has been considered. The damage model is essential to obtain a realistic interfacial shear stress distribution and, therefore, to investigate the diffferent possible failure modes. The following conclusions are drawn from the results of the study:

- The strength and the stiffness of the RC beams strengthened with FRP plates increase, especially for underreinforced beams. The magnitude of the performance is strongly dependent on the axial stiffness of the FRP plate. More FRP axial stiffness implies more increment of the strength and stiffness of the beam.
- It is important to take into account that for beams strengthened with FRP plates of low axial stiffness the strength increase is accompanied by a strong displacement increase which is a phenomenon to consider since non acceptable deflections can be reached under service loads.
- A design approach using the interfacial shear stress as the primary criterion to predict local debonding failure in a strengthened RC beam has been used.
- The interfacial shear stress distribution and, therefore, the location where debonding initiates depends on many factors.
- The use of high axial stiffness plates encourages the end debonding mode since they attract higher axial stresses and, then, high bond stresses.
- Plate length has also an important influence on the debonding mode. Plates located far from the supports tend to maximize the end peel since higher axial stress gradients are produced at the plate end and

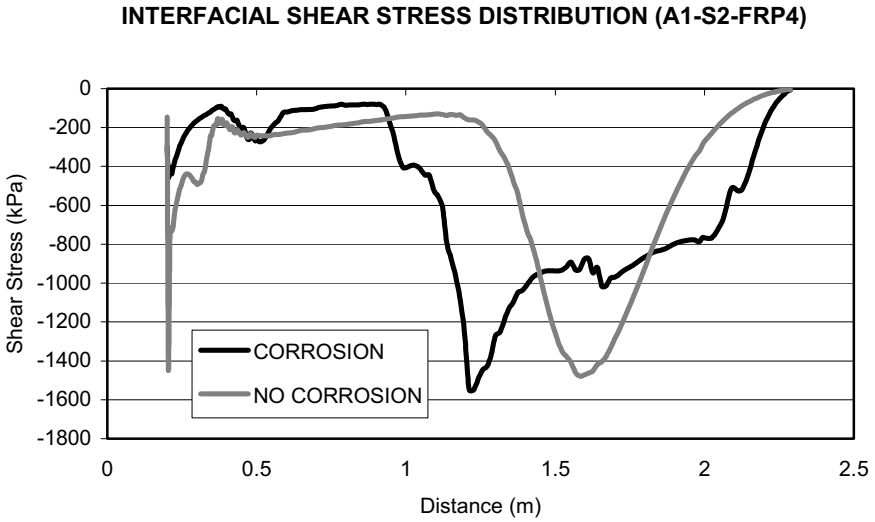

Figure 23 : Variation of shear stress distribution along the concrete/FRP plate interface (Corrosion vs No Corrosion)

therefore the end shear stress is also higher. On the contrary, long plates, located near the supports, tend to minimize end peel.

- There exists also a dependence between the shear stress distribution and the a/h ratio. In general, shallower beams tend to maximize end peel tendencies.
- When strengthening is performed on corroded reinforced concrete beams the effect of corrosion affects especially those beams for which midspan debond occurs.
- It can be remarked that the damage model predicts in a reasonable way the main features of the behavior of a RC beam strengthened with composite plates. For it, a good calibration with experimental results was necessary since it was sensitive enough to the value of the concrete strength.

Acknowledgement: The writer acknowledges support for the work reported in this paper from the Ministry of Science and Technology of Spain (project MAT2000-0971-C02-02).

NOTATION

A_c= Parameter of the damage model (Compression)

A_t= Parameter of the damage model (Tension)

B_c= Parameter of the damage model (Compression)

B_t= Parameter of the damage model (Tension)

d = Damage variable

d_c= Compression damage

d_t= Tension damage

D^e= Elastic moduli

f = Loading surface

t_p= Thickness of the FRP plate

α_c= Weight function (compression)

α_t= Weight function (tension)

ε^e= Elastic strain

ε_{do}= Threshold strain

ε_i= Principal value of the strain

$\tilde{\varepsilon}$ =Equivalent strain

σ =Stress tensor

σ_p= Axial stress of the FRP plate

τ_p= Shear stress of the FRP plate

References

American Concrete Institute (ACI) (2003): Guide for the Design and Construction of Externally Bonded FRP Systems for Strengthenning Concrete Structures, *ACI Manual of concrete practice part 5-ACI 440.2R-02.*

Arduini, M.; Nanni, A. (1997): Parametric Study of Beams Externally Bonded FRP Reinforcements, *ACI Structural Journal* , vol. 94, no. 5, pp 493-501.

Arduini, M.; Nanni, A. (1997): Behavior of precracked RC beams strengthened with carbon FRP sheets,.*Journal of Composites for Construction ASCE,* vol. 1, no. 2, pp 63-70.

Atluri, S. N. (1997): Structural Integrity and Durability, Tech Science Press, Forsyth, GA.

Chajes, M. J.; Finch, W. W.; Januszka, T. F.; Thomson, T. A. (1996): Bond and Force Transfer of Composite Material Plates Bonded to Concrete, *ACI Structural Journal*, vol. 93, no.2, pp 208-217.

Hollaway, L. C.; Leeming, M. B. (1999): Strengthening of Reinforced Concrete Structures, CRC Press, Woodhead Publishing Limited.

Kachanov, L. M. (1958): Time of Rupture Process under Creep Conditions, *Izvestia Akademii Nauk*, USSR, vol. 8, pp 26-31.

Lemaitre, J. (1996): A Course on Damage Mechanics, Springer.

Malek, A. M.; Saadatmanesh, H.; Ehsani, M. R. (1998): Prediction of Failure Load of RC Beams Strengthened with FRP Plate due to Stress Concentration at the Plate End, *ACI Structural Journal*, vol. 95, no.1, pp 142-152.

Mazars, J.; Pijaudier-Cabot, G. (1989): Continuum Damage Theory-Application to Concrete, *Journal of Engineering Mechanics ASCE*, vol. 115, no.2, pp.345-365.

Meier, U.; Deuring, M.; Meier, H.; Schwegler, G. (1993): CFRP Bonded Sheets, A. Nanni (ed) *Fibre-Reinforced-Plastics (FRP) Reinforcement for Concrete Structures: Properties and Applications*, Elsevier Science, Amsterdam.

Mukhopadhyaya, P.; Swamy, N. (2001): Interface Shear Stress: A New Design Criterion for Plate Debonding, *Journal of Composites for Construction ASCE*, vol.5, no.1, pp. 35-43.

Park, J. H.; Ogiso, H.; Atluri, S. N. (1992): Analysis of Cracks in Aging Aircraft Structures, with and without Composite-Patch Repairs, *Computational Mechanics*, vol. 10, pp 169-201.

Rahimi, A.; Hutchinson, A. (2001): Concrete Beams Strengthened with Externally Bonded FRP Plates, *Journal of Composites for Construction ASCE*, vol. 5, no.1, pp. 44-56.

Ravinovich, O.; Frostig, Y. (2000): Closed-form High-Order Analysis of RC Beams Strengthened with FRP Strips, *Journal of Composites for Construction ASCE*, vol. 4, no. 2, pp 65-74.

Ravinovich, O.; Frostig, Y. (2001): Nonlinear High-order Analysis of Cracked RC Beams Strengthened with FRP Strips, *Journal of Structural Engineering ASCE*, vol. 127, no. 4, pp 381-389.

Roberts, T. M. (1989): Approximate Analysis of Shear and Normal Stress Concentrations in the Adhesive Layer of Plated RC Beams, *The Struct. Engr.*, London, vol. 67, no. 12, pp 229-233.

Saadatmanesh, H.; Ehsani, M. R. (1991): RC Beams Strengthened with GFRP Plates. I. Experimental Study, *Journal of Structural Engineering ASCE*, vol. 117, no.11, pp 3417-3433.

Sebastian, W. M. (2001): Significance of Midspan Debonding Failure in FRP-plated Concrete Beams, *Journal of Structural Engineering ASCE* ,vol. 127, no. 7, pp. 792-798.

Sharif, A.; Al-Sulimani, G. J.; Basunbul, I. A.; Baluch, M. H.; Ghaleb, B. N. (1994): Strengthening of Initially Loaded Reinforced Concrete Beams using FRP Plates, *ACI Structural Journal* , vol. 91, no. 2, pp 160-168.

Täljsten, B. (1997): Strengthening of Beams by Plate Bonding, *J. Mat. In Civ. Engrg. ASCE*, vol.9, no.4, pp. 206-212.

Teng, J. G.; Chen J. F.; Smith, S. T.; Lam, L. (2002): FRP Strengthened RC Structures, Wiley.

Triantafillou, T. C.; Deskovic, N. (1991): Innovative prestressing with FRP sheets: mechanics of short-term behavior, *Journal of Engineering Mechanics ASCE* , vol. 117, no. 7, pp 1652-1672.

Wen, T. H., Aliabadi, M. H., Young A. (2002): Boundary Element Analysis of Curved Cracked Panels with Mechanically Fastened Repair Patches, *CMES: Computer Modeling in Engineering & Sciences*, vol. 3, no. 1, pp 1-10.

Zarnic, R.; Gostic, S.; Bosiljkov, V.; Bokan-Bosiljkov, V. (1999): Improvement of Bending Load-bearing Capacity by Externally Bonded Plates, *Proc.Creating with Concrete*, Thomas Telford, London, pp 433-442.